Contrib Mineral Petrol (2007) 153:699–717
DOI 10.1007/s00410-006-0171-7

ORIGINAL PAPER

Deformation-enhanced reaction in experimentally deformed plagioclase-olivine aggregates

A. A. de Ronde · H. Stünitz

Received: 2 March 2006 / Accepted: 27 November 2006 / Published online: 17 January 2007

Abstract The effects of deformation on the kinetics of the net-transfer reaction anorthite + forsterite → cpx + opx + spinel ± gt were studied using static and shear deformation experiments. Experiments were performed on dry anorthite-olivine (An_{92}–Fo_{93}) samples at 900°C and pressures between 1,000 and 1,600 MPa in a Griggs apparatus. Deformed ('non-hydrostatic') and undeformed ('static') samples are compared in terms of phase petrology, reaction rate and reaction mechanisms. Anorthite + olivine reactions are diffusion-controlled as seen from reaction rim structures. In undeformed samples, delayed reaction onset and low reaction rates demonstrate sluggish nucleation of reaction products and slow rates of diffusion at dry conditions, even at 700–900 MPa confining pressure overstepping. The reaction rate is enhanced in deformed An–Fo samples. The higher rate is mainly attributed to a combination of high stresses and viscous deformation processes of the reactants and products, which cause an increase in the nucleation rate of products. The results imply that viscous deformation processes alone can be responsible for the initiation and localisation of metamorphic reactions in dry rocks in the absence of fluid infiltration.

Keywords Plagioclase · Olivine · Viscous deformation · Diffusion-controlled reaction · Reaction kinetics · Nucleation rate

Communicated by T. L. Grove.

A. A. de Ronde was supported by the Swiss National Fond grants 2100-057092.99 and 2000-065041.01.

A. A. de Ronde (✉)
Department of Earth Sciences, University College London, Gower Street, London WC1E 6BT, UK
e-mail: a.deronde@ucl.ac.uk

H. Stünitz
Department of Geosciences, Basel University, Bernoullistrasse 32, 4056 Basel, Switzerland

Introduction

Mineral reactions in deforming rocks play an important role in many tectonic environments because of their influence on the mechanical properties of rocks (e.g. White and Knipe 1978; Rubie 1983; Brodie and Rutter 1987). For example, retrograde reactions in the upper mantle are known to cause strain localisation during the exhumation of upper mantle peridotites (Furusho and Kanagawa 1999; Newman et al. 1999; Handy and Stünitz 2002). Thus, our understanding of how reactions proceed during deformation and which deformation processes tend to enhance reaction are important issues in tectonics.

Mineral assemblages can persist outside their stability conditions if reaction kinetics are sluggish, e.g., due to the absence of aqueous fluids during metamorphism. Metamorphic reactions are often localised in permeable shear zones, while the undeformed surrounding country rocks only show limited or no reaction progress (e.g. Kerrich et al. 1980; Brodie and Rutter 1985; Marquer et al. 1985; Keller et al. 2004). One important reason for enhanced reaction kinetics in high-strain zones is the presence of water because water is an extremely effective catalyst in reaction and mass transport (e.g. Rubie 1986; Austrheim 1987).

Although the initiation and progress of reaction is often attributed to the infiltration of fluids during deformation, for example along micro-fractures or through fine-grained recrystallised rocks (e.g. Austrheim 1987; Früh-green 1994; John and Schenk 2003), there is also the notion that deformation itself may contribute significantly to reaction rates (e.g. Brodie and Rutter 1985; Stünitz 1998).

The effect of viscous deformation processes on reaction in natural shear zones is difficult to assess because the addition of H_2O may obscure the contribution of strain energy during metamorphic reactions. Thus, the effect of deformation on reaction progress without the influence of an aqueous fluid needs to be studied in dry rocks. So far, experimental studies primarily focussed on the effect of viscous deformation on the kinetics of polymorphic transformations (e.g. Davis and Adams 1965; Snow and Yund 1987; Burnley and Green 1989; Kirby and Stern 1993). However, many phase transitions in dry upper mantle and lower crust involve net-transfer reactions with multiple reactants.

The effect of a dry solid–solid reaction on rheology of plagioclase-olivine rocks has been studied recently in shear deformation experiments by de Ronde et al. (2004, 2005). In these experiments, prograde syndeformational reactions between anorthite (An = An_{92}) and olivine (Fo = Fo_{93}) cause mechanical weakening of the An–Fo aggregates at 900°C and 1,000–1,600 MPa pressures. The onset of weakening corresponds to the onset of reaction, and a decrease of differential stress results from grain size reduction by crystallisation of fine-grained (size <0.5 μm) polyphase reaction products. In the sheared An–Fo samples, the greatest reaction progress correlates with the sites of largest strain (de Ronde et al. 2004) and complete reaction is achieved within a relatively short laboratory time scale (de Ronde et al. 2005). Their studies indicate that viscous deformation accelerates reaction between olivine and plagioclase, even under dry conditions. In order to further investigate the potential effect of deformation on the reaction kinetics and rate of a net-transfer reaction in synthetic anorthite-olivine specimens, we have compared our earlier deformation tests (de Ronde et al. 2005), with new tests under hydrostatic loads (i.e. 'static' experiments, 'undeformed' samples) at the same P-T conditions.

Petrology

Anorthite-olivine mineral assemblages are typical for low pressure, high temperature plagioclase peridotites as well as some gabbros. The plagioclase-olivine phase relationships in the $CaO–MgO–Al_2O_3–SiO_2$-system (CMAS) are known from experiments (e.g. Kushiro and Yoder 1966; Green and Hibberson 1970; Jenkins and Newton 1979; O'Neill 1981; Gasparik 1984; Klemme and O'Neill 2000). The equilibrium phase diagram for our An–Fo samples (An_{92}+ Fo_{93}, for detailed compositions see de Ronde et al. 2005) in the system $Na_2O–CaO–FeO–MgO–Al_2O_3–SiO_2$ (NCFMAS) is calculated using the DOMINO-THERIAK software (de Capitani and Brown 1987; de Capitani 1994). These programs use the Berman (1988) database, the plagioclase solution model of Fuhrman and Lindsley (1988), the omphacite solution model of Meyre et al. (1997) and the orthopyroxene model of Hunziker (2003), and take into account fayalite and albite components of olivine and plagioclase. The phase diagram is given in Fig. 1.

The applied confining pressures, P_c, between 1,000 and 1,600 MPa represent different amounts of pressure overstepping of the An–Fo stability field in the NCFMAS-system. At fixed temperature, increasing the pressure corresponds to an increase in Gibbs free energy of the unstable An–Fo assemblage and hence an ex-

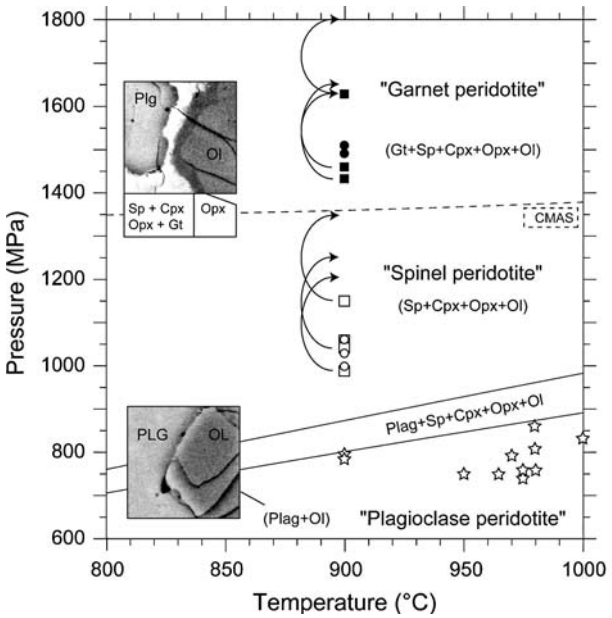

Fig. 1 Phase diagram for plagioclase, spinel and garnet peridotites in the NCFMAS-system. The diagram is calculated for a 0.48 An_{92} + 1.16 Fo_{93} bulk composition (49–51 vol.% An–Fo aggregate) using the program DOMINO. *Stars*: hot pressing conditions inside the plagioclase peridotite stability field. *Circles*: hydrostatic experiments. *Squares*: shear deformation experiments. *Dashed line*: compilation of experimental data of the spinel-garnet peridotite transition (CMAS, see text). *Bottom inset*: detail of stable anorthite-olivine starting material. *Top inset*: Reaction at elevated hydrostatic pressure results in a double-layer reaction rim. *Curved arrows* indicate the maximum mean stress (in MPa) achieved in the deformation experiments. See Table 1 for experimental details

pected increase of the reaction- and nucleation rate. The experiments have been performed in the spinel peridotite and garnet-spinel peridotite fields. In these fields, anorthite (an) and olivine (fo) react to spinel (sp), clinopyroxene (cpx = omphacite), orthopyroxene (opx) and garnet (gt) assemblages, following the reactions

$$an + fo \rightarrow sp + cpx + opx$$

in the spinel peridotite field, and

$$an + fo \rightarrow sp + cpx + opx + gt$$

in the garnet peridotite field.

In our studies, these reactions typically form a two-layer reaction rim (de Ronde et al. 2005): (1) an enstatite (en) layer or 'corona' around olivine porphyroclasts and (2) a rim of mixed fine-grained polyphase reaction products (primarily cpx, opx, sp, ±gt) around anorthite. The structure of the double reaction rim is described as An | (Cpx + Fo + Opx + Sp) | En | Fo, and An | (Cpx + Fo ± Ky + Gt + Opx + Sp) | En | Fo in the spinel and garnet-spinel peridotite field, respectively (Fig. 1).

The formation of an enstatite rim around olivine during reaction between anorthite and olivine (e.g. Joesten 1991; Liu et al. 1997) and olivine and quartz (e.g. Yund 1997; Milke et al. 2001) is attributed to a diffusion-controlled mineral reaction. Diffusion is driven by the gradient of chemical potential between the interacting assemblages and reactions occur principally at the zone boundaries where potential gradients change most rapidly (Fisher 1978). Well-developed mineral zones with sharp zone boundaries are characteristic structures for diffusion-controlled reactions. The rims that formed by syndeformational and hydrostatic reactions in our samples are considered to be diffusion-controlled at a first level of interpretation.

Experimental procedure

Sample assembly

The experiments were performed in a Griggs piston cylinder apparatus using a NaCl-confining medium sample assembly (Fig. 2a). In this assembly, the An–Fo sample is orientated in a shear geometry between two dunite forcing blocks. The temperature of the experiment is measured directly at the sample centre (Fig. 2b).

Starting material

Anorthite–olivine (An–Fo) mixtures were prepared from Åheim dunite olivine (Fo_{93}) and Blumone gabbro anorthite (An_{92}) powders, according to the methods of de Ronde et al. (2005). The powders were stored in an oven at 110°C for at least 72 h ('oven-dried') and were then placed between dunite forcing block pistons. The dunite pistons are 6.3 mm diameter cores of Balsam Gap dunite and Åheim dunite, which are cut at 45° to their cylinder axis. The dunite pistons were thoroughly dried for 12–24 h at 980–1000°C in a $CO–CO_2$ gas mixture.

Dense An–Fo samples were obtained by isostatic hot pressing of the powder mixtures for 24–48 h at high temperatures of 900–1050°C and pressures between 740 and 860 MPa (Figs. 1, 3). These conditions were chosen to keep the assemblage in its stability field during the hot pressing. After hot pressing, anorthite and olivine have a mean initial grain size of 7 ± 2.6 μm and are mixed in a 49–51(±2) volume percent ratio (0.49–1.2 An–Fo molar ratio; Fig. 3). The hot-pressed samples have a porosity of ~2%. No new phases were observed after 48 h of hot pressing (e.g. no melt fractions or other minerals). No reaction products were added to the starting material. The hot pressed samples have a H_2O-content of ±30 ppm (0.003 wt.%), which was determined by measuring the infrared absorption of hydrogen in the olivine of the dunite forcing blocks after the experiments using FTIR (see de Ronde et al. 2005). Thus, the An–Fo samples can be considered as dry mineral samples.

Experiments

All experiments were carried out at 900°C and hydrostatic confining pressures of 1,000–1,600 MPa for the same amount of time as selected deformation experiments (Fig. 1; Table 1). In our earlier tests (de Ronde et al. 2005), the An–Fo samples were deformed with constant shear strain rates ($\dot{\gamma}$) to variable amounts of strain (γ). Table 1 summarises the experiments performed in this study as well as the deformation experiments of de Ronde et al. (2005).

The confining pressure (P_c) inside the sample assembly is maintained by a top lead piece sealing off the assembly. No initial contact exists between the deformation actuator and the top zirconia piston above the jacketed sample (Fig. 2a). In order to start the sample deformation, the force piston first has to travel through the lead until it reaches the 'hit-point' with the top piston and then the sample is subjected to differential stress. Therefore, the total duration of deformation experiments consists of two parts: (1) a static part at constant P_c, in which the force piston advances towards the sample hit-point and (2) the part of actual sample deformation under differential

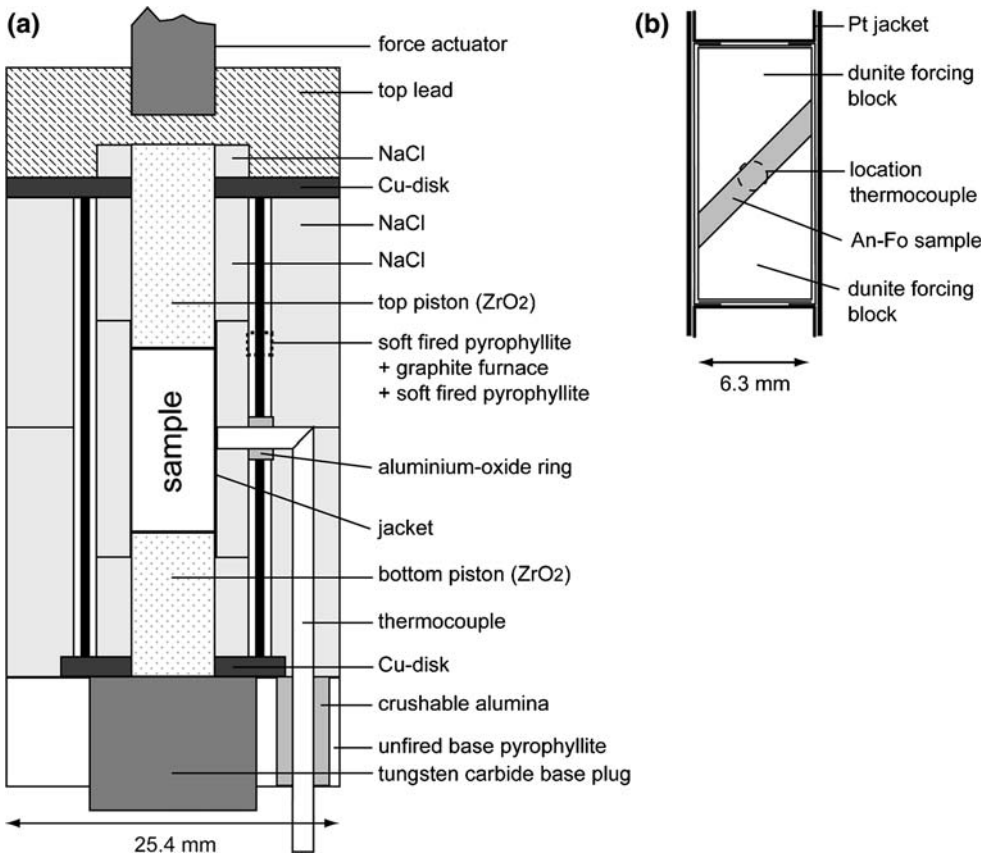

Fig. 2 Schematic diagram of the sample assembly with a solid NaCl-confining medium **a**. The An–Fo sample is placed between two dunite forcing blocks **b**, which are cut at 45° to their vertical axis. The sample + forcing block jacket consists of mechanically-sealed inner Ni-foil and outer weld-sealed Pt tubing

stress. Because both parts occur at pressure outside the An–Fo stability field, the total duration of static experiments has been chosen to be equal to the total duration of the deformation experiments. This time frame allows a direct comparison of the potential reaction period in undeformed and deformed samples. Unfortunately, some small deviations exist between sets of undeformed and deformed samples due to difficulties in reproducing identical confining pressures.

The comparison of deformation and static experiments in terms of time, shear strain, forcing block offset and microstructures is illustrated in Fig. 4a, and is made on the basis of their P_c-value. It needs to be pointed out that the deforming samples are subjected to an additional stress from uni-axial loading. The differential stress σ_d ($\sigma_d = \sigma_1 - \sigma_3$, in which $\sigma_3 = \sigma_2 = P_c$) is difficult to assess on a local grain boundary scale in a polycrystalline aggregate. It is more appropriate to use mean stress σ_m ($\sigma_m = (\sigma_1 + \sigma_2 + \sigma_3)/3$ in which $P_c = \sigma_2 = \sigma_3$) but σ_d values are also mentioned in the text for comparison. The mechanical data of the shear experiments by de Ronde et al. (2005) are summarised in Fig. 4b, as σ_d and $\Delta\sigma_m$ ($\Delta\sigma_m = \sigma_m - P_c$) versus shear strain ($\gamma$). The effect of stress on the P_c-overstep of the experiments will be addressed in the Discussion.

Sample examination

Thin sections were prepared normal to the sample-forcing block interface and parallel to the shear direction. The samples were studied in backscattered imaging mode (BSEM) using an EDS-equipped environmental scanning electron microscope. An EDS-equipped transmission electron microscope (TEM) was used at 200 kV acceleration voltage to identify the mineral assemblages of sub-micron sized reaction products and to obtain information on grain sizes and dislocation microstructures of all phases. The volume percentages of anorthite, olivine and reaction products were estimated from their area percentages in thin section (Underwood 1970). The area percentages of the phases were obtained by detailed tracing of phase boundaries as well as thresholding of phases in high quality mosaics of four BSEM-images of the samples with 1,600 × magnification. Errors in the volume percentages due to tracing are ca. ±1% and the error in the mean volume percentages is ±2%.

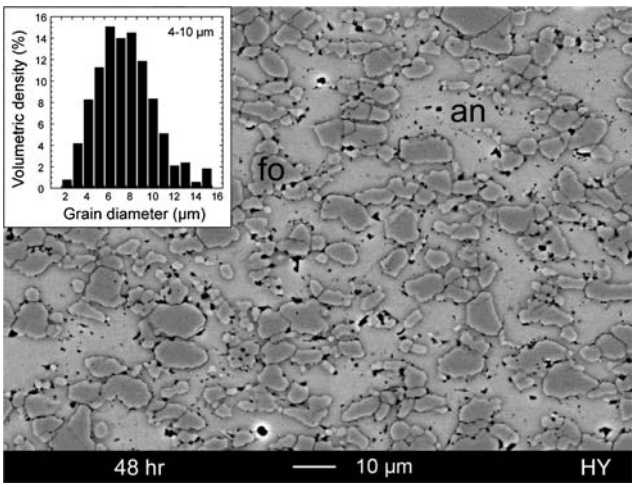

Fig. 3 Backscattered scanning electron microscope (BSEM) image of An–Fo sample 44AA after 48 h hot pressing at 965°C and 750 MPa. Phases: anorthite (an = An_{92}, *light grey*, low relief), olivine (fo = Fo_{93}, *dark grey*, high relief). Average An–Fo vol.% ratio = 49–51 (±2)%. The initial mean grain size of olivine and presumably plagioclase is 6.9±2.6 µm. Sample porosity and holes ~2% (*black*). White rims are due to charging of the sample

The stable reaction product assemblages partially consist of olivine (Fig. 1). Hence, complete reaction is characterised by total disappearance of anorthite from the sample whereas some olivine remains. The reaction progress ξ, is defined as the amount of anorthite transformation,

$$\xi = 1 - \frac{V_{\mathrm{An_{residual}}}}{V_{\mathrm{An_{initial}}}} = 1 - \frac{V_{\mathrm{An_{residual}}}}{49}$$

which describes the volume fraction of transformed anorthite with respect to the initial An–Fo sample.

Experimental results

The microstructures of samples in the spinel and garnet peridotite field are distinguishable in terms of reaction progress. Therefore, we will describe microstructures for each field separately and we refer to the spinel and garnet peridotite experiments as low (~300 MPa) and high (~800 MPa) P_c-overstepping experiments, respectively.

Low P_c-overstepping (~300 MPa)

Static experiments

In a time span of 73 h, reaction does not take place in static experiments at 1,060 MPa (Fig. 5a). Reaction

Table 1 Summary of anorthite–olivine experiments at 900°C

Run	Hot pressing			Hydrostatic[a]		Deformation[b]						Volume phases (%) [c]				
No.	T (°C)	P_c (MPa)	t (h)	P_c (MPa)	t_{hy} (h)	$\dot{\gamma} \cdot 10^{-5}$ (s^{-1})	γ	σ_m^{max} (MPa)	σ_d^{max} (MPa)	t_{de} (h)	t_{total} (h)	An	Fo	En	Other	ξ
Hydrostatic experiments																
44AA	965	750	48					750	0		48.0	49	51	0	0	0.00
W1046	1050	760	24	1,000	19.0			1,000	0		19.0	51	49	0	0	0.00
36AA	970	790	48	1,030	168.0			1,030	0		168.0	43	47	←	10	0.12
47AA	975	740	48	1,060	73.3			1,060	0		73.3	45	55	0	0	0.00
W1045	900	790	24	1,490	30.0			1,490	0		30.0	46	54	0	0	0.00
34AA	950	750	48	1,510	167.5			1,510	0		167.5	13	31	21	35	0.73
49AA	975	760	48	1,510	59.0			1,510	0		59.0	36	49	←	15	0.27
Deformation experiments																
W1028[d]	1050	780	24	990	12.5	4.9	4.1	1,205	640	23.3	35.8	45	48	←	7	0.08
19AA	1000	830	24	1,160	37.0	4.7	5.9	1,346	560	35.0	72.0	17	21	19	43	0.65
17AA	1000	771	24	1,435	35.3	4.6	4.5	1,648	639	27.2	62.5	10	26	24	40	0.80
32AA	980	760	48	1,460	22.8	3.8	2.2	1,642	521	15.9	38.7	33	48	←	19	0.33
28AA	980	860	48	1,630	26.8	4.0	4.9	1,812	521	34.0	60.8	2	21	23	54	0.96
Combined deformation and hydrostatic experiments[e]																
33AA	980	810	48	1,030	22.2	4.3	5.8	1,250	660	37.7	163.9	11	19	22	48	0.78
52AA	965	730	48	1,480	33.5	3.9	2.5	1,689	627	17.4	393.9	9	25	25	41	0.82

Run numbers in *italic* are experimental data of de Ronde et al. (2005)

[a] t_{hy}: duration at hydrostatic confining pressure (P_c)

[b] t_{de}: duration of 'sample deformation' at differential stress; $t_{total} = t_{hy} + t_{de}$; $\sigma_m = (\sigma_1 + \sigma_2 + \sigma_3)/3$, with $\sigma_2 = \sigma_3 = P_c$; $\sigma_d = P_c - \sigma_1$

[c] Estimated vol.% of reactants and reaction rims. ← : enstatite rim was not resolved, possibly part of the Fo vol.%

[d] The γ-value is less than depicted due to forcing block deformation (de Ronde et al. 2005)

[e] The applied load in these two experiments was removed within 1 h after deformation. Samples were then kept at hydrostatic P_c for 104 h at P_c = 1,040 MPa (33AA) and 343 h at P_c =1,470 MPa (52AA)

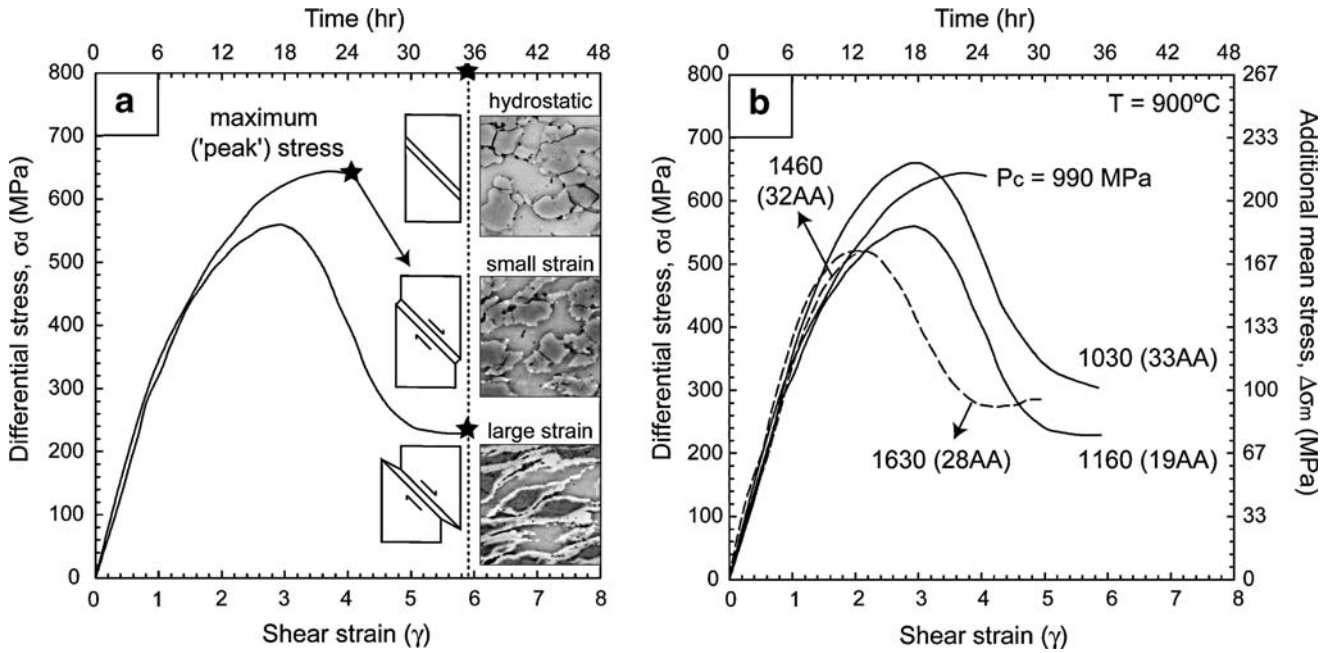

Fig. 4 Mechanical data for shear deformation experiments on An–Fo aggregates at 900°C. **a** Example set of static and deformation experiments. Small forcing block offset produces small strain (top curve + middle inset) and few reaction products are observed in the sample (*white spots*). Larger offsets produce larger strain (bottom curve + inset) deforming extensively the An–Fo aggregate, which has now reacted (*white rims*). During hydrostatic loading at same time scales there is no offset of forcing blocks (*top inset*) and no reaction. **b** Differential stress ($\sigma_d = \sigma_1 - P_c$) versus shear strain ($\gamma$) for experiments in the spinel peridotite (*solid lines*) and the garnet peridotite (*dashed lines*) field (modified after de Ronde et al. 2005). Labels indicate the confining pressure (P_c) and the sample number. The right axis displays the ''additional'' mean stress, $\Delta\sigma_m$. ($\Delta\sigma_m = \sigma_m - P_c$, in which $\sigma_m = (\sigma_1 + \sigma_2 + \sigma_3)/3$ and $P_c = \sigma_2 = \sigma_3$). Deformation of An–Fo samples results in strain hardening followed by strain weakening towards the onset of a constant σ_d of ~280 MPa at $\gamma \sim 5.0$

products are only observed in an undeformed sample kept for 168 h at P_c = 1,030 MPa (Fig. 5b). Small patches of fine-grained products occur at the olivine-plagioclase boundaries throughout the entire sample (ξ = 0.12), but no continuous reaction rims form. The time required for the onset of reaction, i.e. for the nucleation of the first new phases, under hydrostatic and low P_c-overstepping conditions is not well constrained in the data presented here but lies between 73 and 168 h. This delayed onset of reaction and the patchy distribution of products indicate that nucleation and growth of new phases is difficult in these dry samples. An enstatite rim could not be observed properly below ξ = 0.10 because of its small scale.

Deformation experiments

Samples deformed in shear under differential stresses show a remarkably higher reaction progress than undeformed samples. Deformation to peak stress conditions (σ_m^{max} = 1,205 MPa, σ_d^{max} = 640 MPa) in 36 h at P_c = 990 MPa results in a reaction progress of ξ = 0.08 (Fig. 5c). Small patches of products on the anorthite-olivine phase boundaries are homogeneously distributed throughout the sample and show no preferred orientation. The slightly elongate grain shapes of anorthite as well as the weak alignment of reactants along the extension direction (Fig. 5c) indicate some crystal plastic flow to small strain. The observed reaction progress is similar to that of the 168 h undeformed sample at P_c = 1,030 MPa (Fig. 5b). The onset of reaction must be triggered by deformation or applying load to the samples because no reaction products form within 36 h in static experiments at 1,060 MPa (Fig. 5a).

Shear deformation of samples to large strain ($\gamma > 3$) is characterised by an initial increase of σ_m to a maximum followed by a significant mechanical weakening (i.e. a reduction in σ_m, Fig. 4). The anorthite-olivine aggregate deformed to γ = 5.9 at P_c = 1,160 MPa displays extensive reaction (ξ = 0.65; t_{total} = 72 h; Fig. 5d). A maximum σ_m of 1,347 MPa (σ_d^{max} = 560 MPa) was obtained during this experiment (Fig. 2b). It is striking that the reaction progress is more than five times higher than that of the undeformed sample at P_c = 1,030 MPa for 168 h (ξ = 0.12). An undeformed sample at P_c = 1,060 MPa for the same period of time shows no reaction products (Fig. 5a).

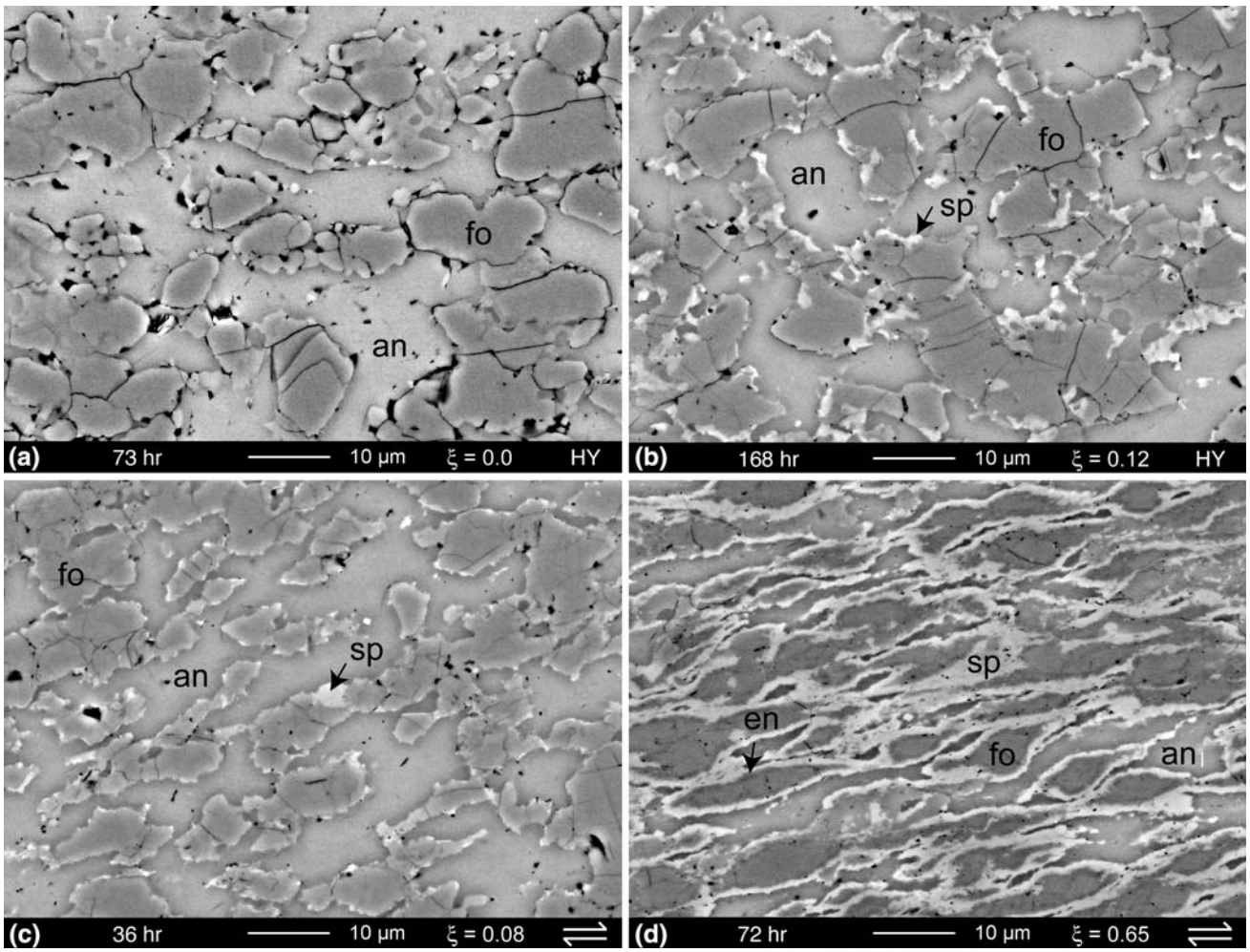

Fig. 5 Microstructures of An–Fo aggregates in the spinel peridotite field (BSEM). Phases: fo (olivine), an (anorthite), sp (opx + cpx + spinel), en (enstatite rim). **a** Undeformed sample 47AA at P_c = 1,060 MPa for 73.3 h. Reaction did not take place. **b** Undeformed sample 36AA at P_c = 1,030 MPa for 168 h. Discontinuous reaction rims are characterised by randomly distributed patches of products at the anorthite-olivine interfaces. **c** At P_c = 990 MPa, syndeformational products formed in sample W1028 during deformation to peak stress conditions in 35.8 h (σ_d^{max} = 640 MPa, σ_m^{max} = 1,205 MPa). **d** Sample 19AA deformed to γ = 5.9 at P_c = 1,160 MPa in 72 h (σ_d^{max} = 560 MPa, σ_m^{max} = 1,347 MPa) is characterised by strongly deformed anorthite and olivine grains and extensive reaction. The bright fine-grained reaction products have coalesced and form layers across the sample. An enstatite rim is visible around olivine grains

Deformation in the samples is partially accommodated by dynamic recrystallisation of olivine and anorthite de Ronde et al. (2005). During dynamic recrystallisation, dislocations in anorthite and olivine grains are partially arranged into dislocation walls (formation of subgrains). Subgrain rotation and migration of grain boundaries (e.g. grain boundary bulging) produce new recrystallised grains. As a result, the deformed anorthite and olivine grains are elongated and have fine-grained recrystallised tails (Figs. 5d, 6a).

The samples deformed to large strain are characterised by a continuous layer (width ~0.8 μm) of reaction products around anorthite grains as well as thin (width ~0.6 μm) enstatite rim around olivine grains (Fig. 5d). Shear deformation of the reaction products around anorthite produces interconnected layers across the sample. As a result, the geometry of the two-layer reaction rim is somewhat complex in the deformed samples. The reaction products have accommodated most of the strain in the interconnected layers by granular flow (i.e. small grains to slide past each other by non-frictional grain boundary sliding, de Ronde et al. 2005). Enstatite grains in the rim around olivine have remained around olivine porphyroclasts and do not coalesce (Fig. 5d). The presence of corona structures and the smooth interface between the enstatite rim and olivine suggest that reaction between anorthite and olivine is diffusion-controlled.

One experiment has been performed to test to the rate of reaction if an initial period of deformation is followed by a period of hydrostatic pressure. In this experiment, large strain deformation ($\gamma = 5.8$) at P_c of 1,040 MPa is followed by a 104 h period of hydrostatic P_c of 1,030 MPa. Hydrostatic pressure is achieved by removing the differential stress from the sample after deformation by rapid retraction of the σ_1 piston (within 1 h). Despite the long period at low P_c-overstepping conditions (~164 h, including deformation to σ_m/σ_d of 1,250/660 MPa), the reaction is not completed ($\xi = 0.78$). Remnants (size ~2 μm) of deformed anorthite grains are still observed throughout the entire sample (Fig. 7). The main difference between this sample and the deformed ones is the granular microstructure of much coarser-grained products (size up to 2 μm) and considerably thicker enstatite rims (width ~2 μm) around olivine after the hydrostatic treatment (Fig. 7). Thus, after initial nucleation of products during the deformation period, the product grains appear to grow during the hydrostatic treatment without much further nucleation.

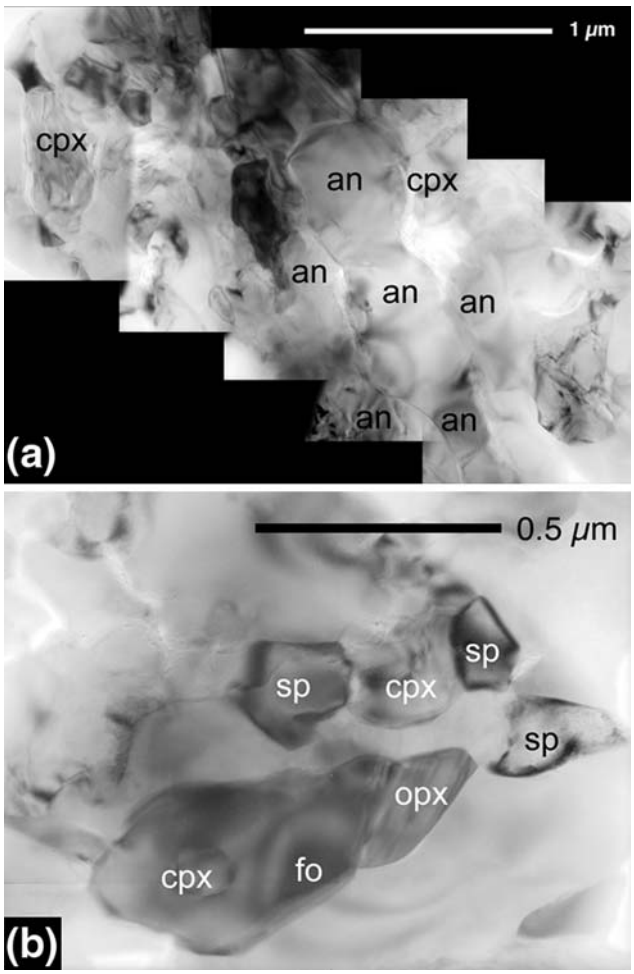

Fig. 6 Microstructures of deformed An–Fo aggregates in the spinel peridotite field (bright-field TEM). **a** Small dislocation-free anorthite grains (an; size ~0.25 μm) make up the tails of the elongated anorthite grains in Fig. 5d. These small unstable anorthite grains occur directly adjacent to newly formed cpx. **b** Detail of fine-grained (size ~0.25 μm) syndeformational reaction products (Fig. 5d). The mineral assemblage consists of clinopyroxene (cpx), orthopyroxene (opx) and spinel (sp). The products are dominantly dislocation-free

Reaction products

The syndeformational reaction products that form in the spinel peridotite field samples are identified as orthopyroxene (opx), clinopyroxene (cpx) and spinel (Fig. 6b). The new phases are fine-grained (size ~0.25 μm) and dislocation-free. Small enstatite grains occur dispersed between all other reaction products. Aggregates of ~0.25 μm anorthite grains (formed by dynamic recrystallisation) are present after deformation at $P_c = 1{,}160$ MPa (Fig. 6a). The formation of these small unstable anorthite grains adjacent to new reaction products emphasises that diffusion processes in these samples must be very slow.

High P_c-overstepping (~800 MPa)

Static experiments

In static experiments, reaction in the garnet peridotite field starts earlier than in the spinel-field. A continuous two-layer reaction rim forms (width ~0.8 μm) at the An–Fo interphase boundaries after 59 h at $P_c = 1{,}510$ MPa ($\xi = 0.27$, Fig. 8a). In contrast, reaction at low P_c-overstepping does not start after this period, indicating that the greater P_c-overstep at $P_c = 1{,}510$ MPa promotes the nucleation of products and the rate of reaction. At $P_c = 1{,}510$ MPa, reaction has progressed to $\xi = 0.73$ after 168 h (Fig. 8b) and can be almost complete at a few locations in the sample. The reaction product grains are relatively coarse-grained (size >1 μm) and have either a blocky or fibrous microstructure (Fig. 9a).

Deformation experiments

In the An–Fo sample deformed to the onset of mechanical weakening at $P_c = 1{,}460$ MPa ($\gamma = 2.2$, $\sigma_m^{max} = 1{,}634$, $\sigma_d^{max} = 521$ MPa), reaction has progressed considerably further ($\xi = 0.33$, Fig. 8c) compared to the sample deformed at $P_c = 990$ MPa ($\xi = 0.08$, Fig. 5c) during approximately the same time (39/36 h). Thin continuous rims of reaction products (width ~1 μm) are formed along all An–Fo interphase boundaries. The original anorthite and olivine grains

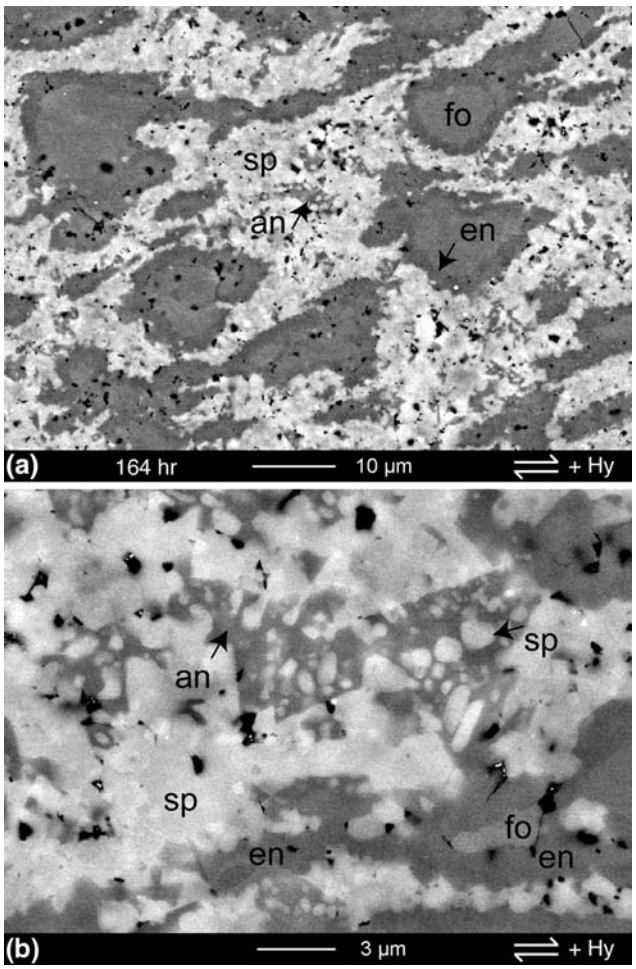

Fig. 7 Microstructure of sample 33AA after a combined deformation and hydrostatic pressure experiment at P_c = 1,030 MPa (BSEM). Deformation to $\gamma = 5.8$ (σ_d^{max} = 660 MPa, σ_m^{max} = 1,250 MPa) was followed by an additional 104 h at hydrostatic pressure (t_{total} = 163.9 h; $\xi = 0.78$). Phases: fo (olivine), an (anorthite), sp (opx + cpx + spinel), en (enstatite rim). **a** Thick ~1–2 µm enstatite rims formed. The sp-reaction product matrix has a granular microstructure. Internal rim structures are obliterated. **b** Detail of the reaction product matrix. New phases are coarser-grained (sizes up to ~1.5 µm) and grow into the crystal plastically deformed anorthite grains (Fig. 5d)

are slightly deformed, producing a weak shape preferred orientation. Both reactants have local high dislocation densities and poorly organised dislocation walls typical for deformation at high stresses (i.e. low temperature plasticity, de Ronde et al. 2005).

Distinctively different reaction product microstructures form at large strain and high reaction progress. After deformation to $\gamma = 4.9$ at P_c = 1,630 MPa (σ_m^{max} = 1,804 MPa, σ_d^{max} = 521 MPa), most of the sample consists of relict olivine grains embedded in a fine-grained reaction product matrix (Fig. 8d). This nearly complete reaction during shear deformation is achieved in just 61 h ($\xi = 0.96$), whereas only thin continuous reaction rims have developed in the undeformed sample after 59 h at P_c = 1,510 MPa (Fig. 8a).

After deformation to large strain, fine-grained enstatite rims form tails at relict olivine porphyroclasts inside the other reaction products (Fig. 8d). The enstatite rims have more irregular and lobate shapes (Fig. 9b), suggesting that enstatite grains are partially removed from the growing enstatite rim by granular flow. The reaction products between the relict olivine clasts are finer-grained (sizes ~0.1–0.5 µm) than those in the P_c = 1,510 MPa undeformed sample (Fig. 9a, b) indicating more rapid nucleation during syndeformational reaction.

Reaction products

The syndeformational products after large strain at P_c = 1,630 MPa (σ_m^{max} = 1,804 MPa, σ_d^{max} = 521 MPa), are identified as opx, cpx, spinel, garnet and kyanite (Fig. 10). The products are dominantly dislocation-free and heterogeneously mixed (Fig. 10a). The presence of kyanite deviates from the calculated equilibrium assemblage for garnet peridotites in the NCFMAS-system (Fig. 1) regardless of an increased σ_m or σ_d. The needle-shaped kyanite grains (~1 µm long, Fig. 10b) only occur in the internal parts of the reaction product matrix and are absent in a ~1.5 µm wide zone directly adjacent to enstatite rims (Fig. 9b). Kyanite is absent in the low strain samples, suggesting that it formed at large shear strains ($\gamma > 3$, $\Delta\sigma_m < 150$ MPa) and higher reaction extent ($\xi > 0.33$).

The enstatite rims are characterised by fine-grained (size <0.5µm) opx grains directly adjacent to relict olivine. Larger olivine grains frequently display dislocation walls, indicating dislocation creep (Fig. 10c). Sporadic dislocation arrays in some newly formed pyroxene grains with ~0.5 µm grain size also indicate dislocation creep. However, the majority of the products are finer-grained and free of dislocations, suggesting that the products dominantly accommodate deformation by granular flow. In the low strain sample deformed to a σ_m^{max} of 1,804 MPa at P_c = 1,460 MPa ($\gamma = 2.2$; σ_d^{max} = 512 MPa, Fig. 8d), cpx, spinel and garnet are typically observed as small grains (size 0.1–0.5 µm) at sites of high dislocation densities in relict grains (Fig. 10d).

Reaction rates

The effect of shear deformation on the reaction rate and the differences between undeformed and deformed samples is clearly illustrated by plotting reac-

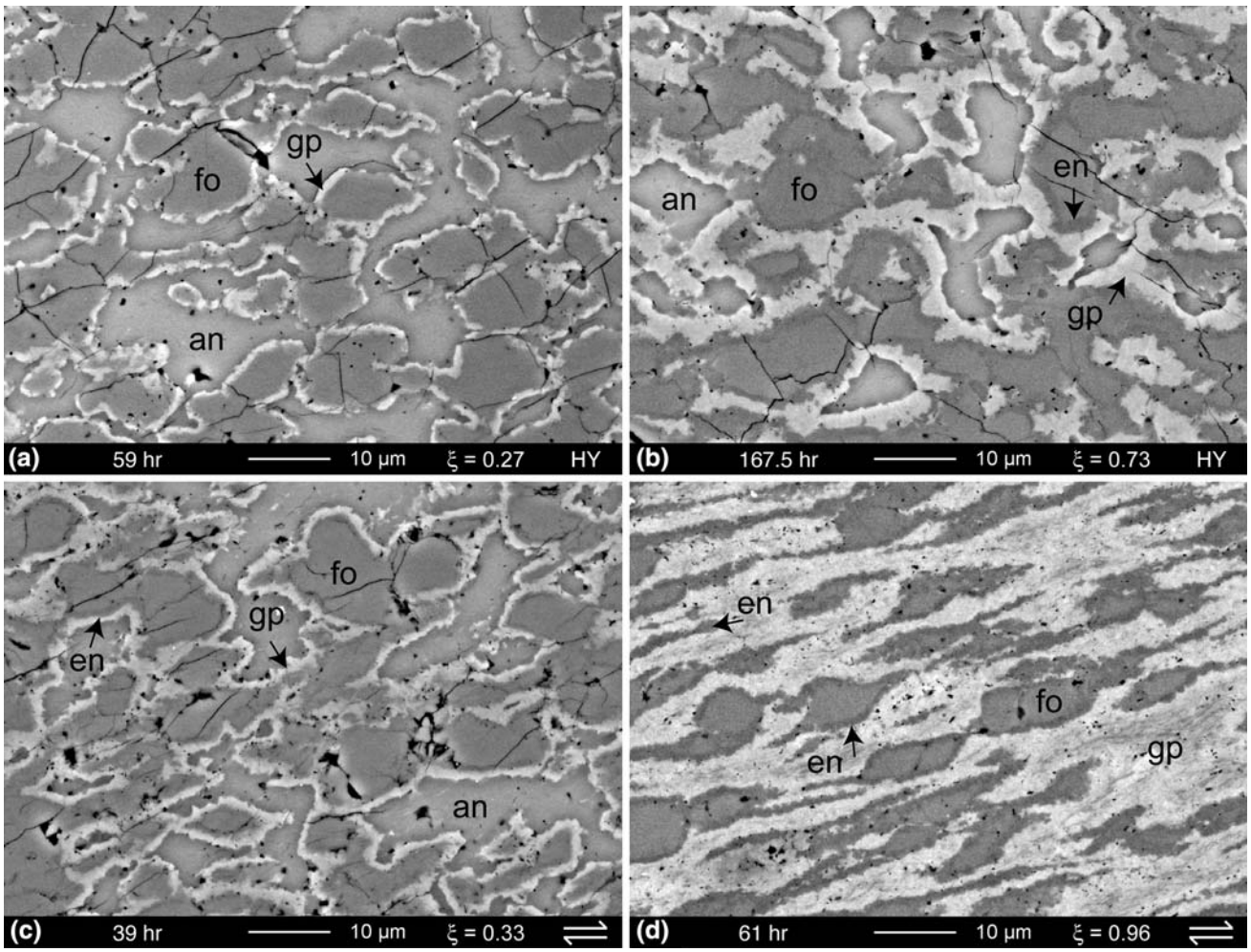

Fig. 8 Microstructures of An–Fo aggregates in the garnet peridotite field (BSEM). Phases: fo (olivine), an (anorthite), gp (opx + cpx + spinel + garnet ± kyanite), en (enstatite rim). **a** Undeformed sample 49AA at P_c = 1,510 MPa for 59 h. **b** Undeformed sample 34AA at P_c = 1,510 MPa for 167.5 h. The pronounced two-layer reaction rim indicates a diffusion-controlled reaction. **c** Sample 32AA deformed to γ = 2.2 and peak stress (σ_d^{max} = 521 MPa, σ_m^{max} = 1634 MPa) at P_c = 1,460 MPa (t_{total} = 39 h). The aggregate grains developed a weak shape preferred orientation. Olivine grains have a thin (width ~1.0 μm) continuous enstatite rim. Bright reaction products form a continuous rim around anorthite. **d** Sample 28AA deformed to γ = 4.9 at P_c = 1,630 MPa in 61 h (σ_d^{max} = 521 MPa, σ_m^{max} = 1,804 MPa). The An–Fo reaction is near complete in the centre of the sample shear zone. Relict olivine grains are embedded in a bright matrix of reaction products. The two-layer rim structures are obliterated. Olivine grains have rims and tails of fine-grained enstatite

tion progress ξ versus time (Fig. 11). The undeformed sample at P_c ~ 1,000 MPa in the spinel field only shows 12% reaction progress after 168 h. In contrast, reaction progress in deforming samples with an average σ_m ~ 1,200 MPa is 65% after 72 h (Fig. 11a). The maximum σ_m is 1,270 MPa on average, which is maintained for about 25% of the total duration of the experiment (Fig. 4b). The reaction rate in the deforming samples varies somewhat between the individual experiments but the mean reaction rate is ~0.02 ξh^{-1}.

At greater P_c-overstep in the garnet peridotite field, the difference between deformed and undeformed samples is less pronounced but still present. Reaction progress at hydrostatic P_c of 1,510 MPa is consistent with an exponential relationship with time (Fig. 11b), resulting in ξ ~ 75% after 168 h. The syndeformational reaction rate is higher and appears to be linear with time. The deformation experiments have an average $\Delta\sigma_m$ of 120 MPa, with σ_m^{max} ranging from 1,630 MPa to 1,800 MPa for the P_c = 1,460 and 1,630 MPa experiments, respectively. Above average mean stress was measured at γ ~ 1.5 to 3 (i.e. ~10 h; Fig. 4b). Near-complete reaction is obtained in less than 35 h of deformation, indicating a reaction rate of ~0.03 ξh^{-1} (Fig. 11b).

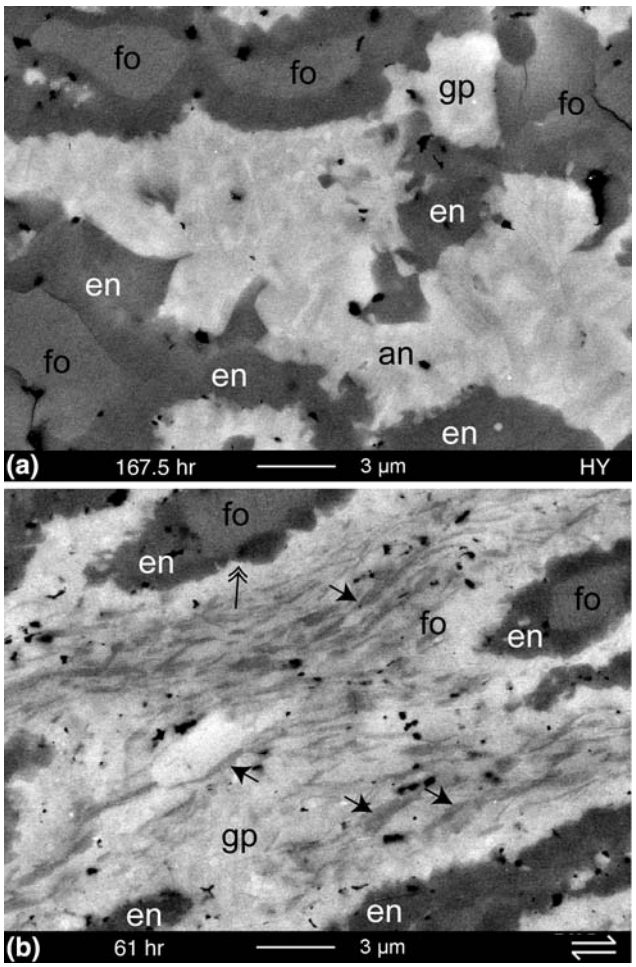

Fig. 9 Representative microstructures of reaction products in the garnet peridotite field (BSEM). Phases: fo (olivine), an (anorthite), gp (opx + cpx + spinel + garnet ± kyanite), en (enstatite rim). **a** The bright reaction product matrix in this undeformed sample is coarse-grained and has a needle-like microstructure after 167.5 h at P_c = 1,510 MPa (Fig. 8b; sample 34AA). Enstatite rims are pronounced. The en-fo interface is smooth. **b** The matrix of syndeformational products in sample 28AA deformed to γ = 4.9 at P_c = 1,630 MPa (σ_d^{max} = 521 MPa, σ_m^{max} = 1,812 MPa) contains elongate dark kyanite (*single arrows*). Enstatite rims around olivine are continuous but have an irregular, lobate appearance (*double arrows*), indicating displacement of products by granular flow

In order to further study the effect of deformation on reaction, the change in reaction rate was estimated for the two experiments in which the samples were first deformed and then kept at hydrostatic pressure (samples 33AA and 52AA, Table 1). Hydrostatic pressure was achieved by quickly removing differential stress after deformation. The reaction rate in the static part was determined by measuring ξ after the static period and by assuming that the ξ of the deformation part is the same as that of a sample deformed to similar γ at similar P_c and σ_m (Fig. 11).

The samples of these combined deformation-static experiments display a fast initial reaction rate during deformation (at higher mean stress), followed by a reduced reaction rate at hydrostatic pressure (at lower mean stress). In the low P_c-overstepping experiments (Fig. 11a), the reaction rate approximately decreases from 0.02 to 0.001 ξh^{-1} (assuming a comparable ξ after deformation to γ = 5.8 at P_c = 1,030 MPa and γ = 5.9 at P_c = 1,160 MPa). A similar trend is observed in the high P_c-overstep experiments (Fig. 11b), in which the reaction rate is reduced from 0.03 ξh^{-1} to ~0.001 ξh^{-1} (assuming a comparable ξ after deformation to γ = 2.2 and P_c = 1,460 MPa and γ = 2.5 and P_c = 1,480 MPa). The change in $\Delta\sigma_m$ from the deformation part to the static part is approximately 200 and 190 MPa for the low and high P_c-overstep experiments, respectively. Hence, in these combined deformation-static experiments, the syndeformational reaction rate is about one order of magnitude greater than the static one, similar to the difference between deformation and static experiments.

Discussion

In summary, it is evident from all experiments that deformation accelerates the reaction between anorthite and olivine. The acceleration is most clearly expressed by the earlier onset of reaction and an overall higher reaction rate in the deformed samples compared to undeformed ones. The effect is also demonstrated by the decrease in reaction rate when viscous deformation processes are stopped by removing the differential stress from the sample. In order to discuss the causes for the deformation-enhanced reaction, we will first summarise the conditions and mechanisms of static reaction and then discuss potential processes that may lead to faster reaction kinetics in the deformed samples.

Diffusion-controlled reactions

The two-layer reaction rim microstructures in the undeformed samples are characteristic for diffusion-controlled reactions. The approximate exponential decrease of reaction rate with time is likely to reflect the decrease in the gradient of chemical potential between the reactants that drives the reaction. In comparison to other kinetic studies on diffusion-controlled reactions (e.g. Liu et al. 1997; Milke et al. 2001), the growth rate of reaction rims in undeformed An–Fo samples is slower. Liu et al. (1997) have measured a 5.5 μm thick rim (X^2~ 30 μm) after approximately 140 h at 1000°C

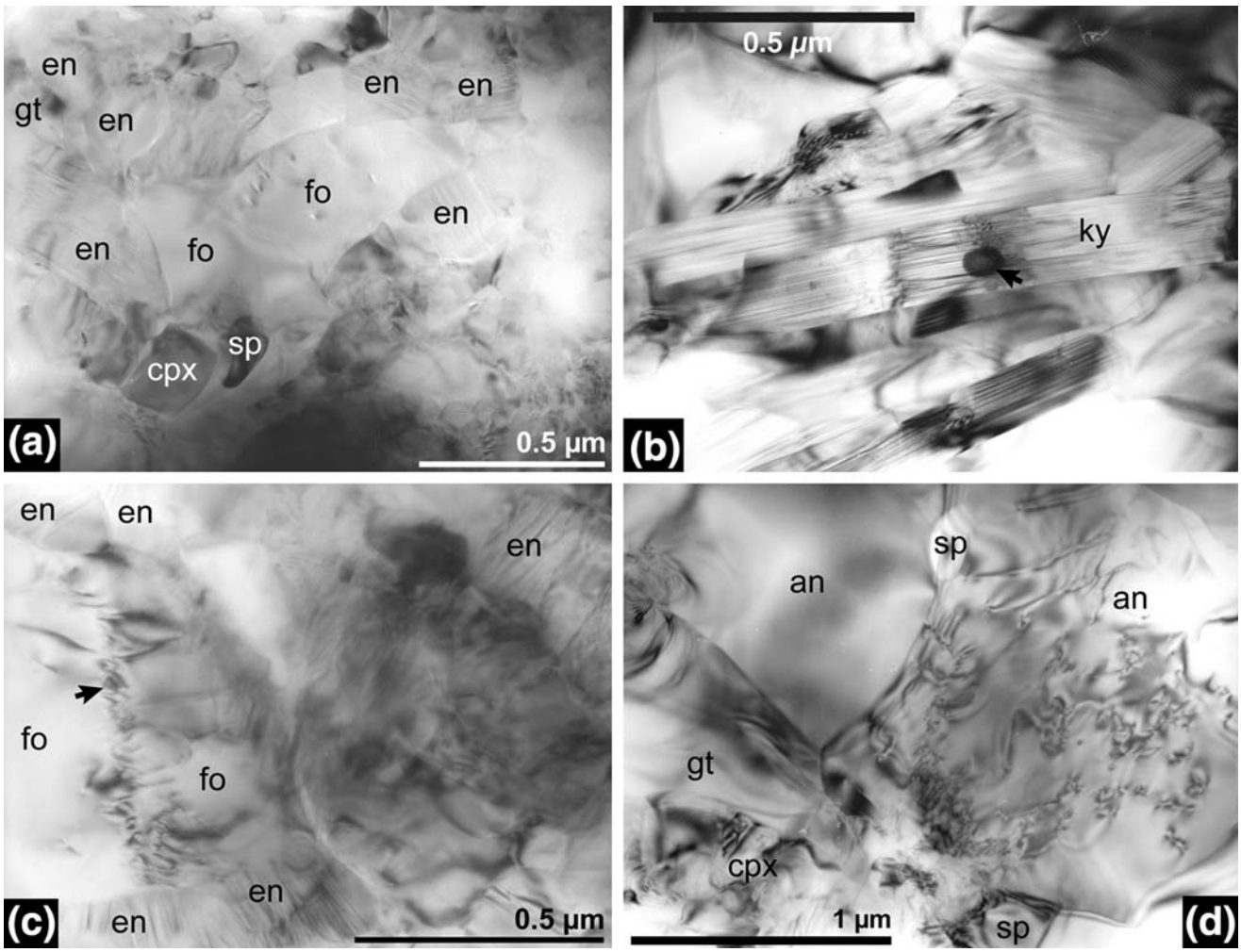

Fig. 10 Representative microstructures of syndeformational reaction products in the garnet peridotite field (bright-field TEM). **a** Reaction product assemblage: spinel (sp), orthopyroxene (en), clinopyroxene (cpx) and garnet (gt) together with small <0.5-µm forsterite-rich olivine grains (fo). The products are dominantly dislocation-free. **b** Needle-shaped kyanite (ky) at $\gamma = 4.9$ and $P_c = 1{,}630$ MPa (28AA). The *dark spot* inside the grain indicates the size of an EDS analysis. **c** Detail of 0.25-µm orthopyroxene grains (en) adjacent to a small relict olivine grain (fo). The olivine grain contains a disordered dislocation wall (*arrow*). **d** Garnet (gt), spinel (sp) and clinopyroxene (cpx) formed adjacent to an anorthite grain (an) with a high dislocation density after $\gamma = 2.2$ at $P_c \sim 1460$ MPa (32AA; $\sigma_d^{max} = 521$ MPa, $\sigma_m^{max} = 1{,}634$ MPa). Also note the low dislocation density of the anorthite grain in the top left

and P_c =700 MPa in vacuum dried (250°C) olivine-anorthite samples and deduced a parabolic rate constant of k ~ 0.25 µm^2 h^{-1}. Our low P_c-overstep samples display reaction rims less than 1 µm thick ($X^2 < 1$ µm) at 900°C and P_c =1,030 MPa after 168 h (Fig. 5b). This difference of one order of magnitude in rim thickness suggests that it probably is not only the 100°C lower temperature, but also the lower water content of our samples that is responsible for the limited rim growth. Unfortunately, it is difficult to determine the diffusion rate controlling components in our samples because the observed rim structures may not represent a steady-state configuration (Joesten 1978; Liu et al. 1997) and the phase compositions of the fine-grained products cannot be resolved quantitatively.

The limited rates of diffusion at water-deficient conditions are clearly demonstrated in the deformed samples as well. First of all, it is observed that fine-grained anorthite can persist locally on a very small scale at 1,000 MPa (Fig. 6a). Even though anorthite is unstable, local dynamic recrystallisation at certain places is not associated with a change in composition. In such cases, the driving potential for recrystallisation is solely due to the deformational energy stored in the crystals (in the

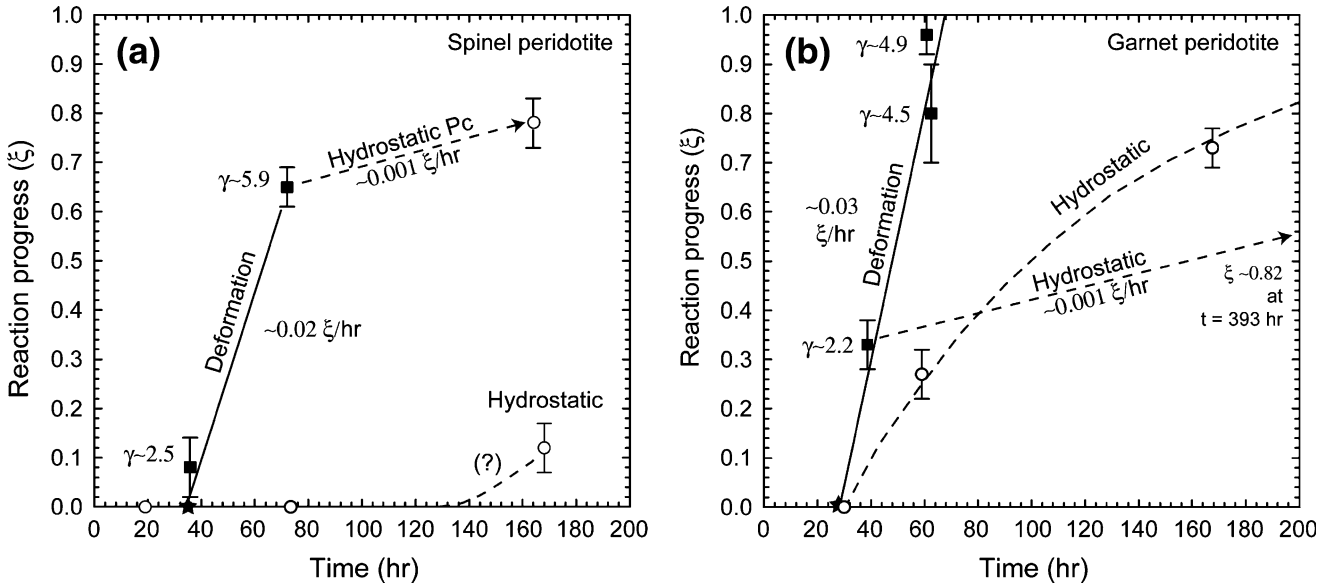

Fig. 11 Reaction progress ξ versus time for static (*circles*) and shear deformation experiments (*squares*). Labels are γ-values of the experiments. *Lines* indicate the overall trend of reaction in deformed (*solid*) and static (*dotted*) samples. Error bars are the standard error in mean vol.% of the measured An vol.%. *Stars* indicate the onset of deformation. **a** Spinel peridotite field. The estimated syndeformational reaction rate is ~0.02 ξh^{-1}. The onset of reaction at hydrostatic pressure is unknown (*bottom line*). The *dotted arrow* indicates an estimate of the reaction rate at hydrostatic P_c of 1,030 MPa when deformation was stopped at $\gamma \sim 5.9$ (σ_d^{max} = 660 MPa, σ_m^{max} = 1,250 MPa). **b** Garnet peridotite field. The estimated syndeformational reaction rate is ~0.03 ξh^{-1}. The reaction rate in undeformed samples is consistent with an exponential relationship (curve fit is ξ_{hy}= 1-exp(0.3-0.01t)). The *dotted arrow* indicates an estimate of the reaction rate at hydrostatic P_c of 1,480 MPa when deformation was stopped at $\gamma \sim 2.5$ (σ_d^{max} = 627 MPa, σ_m^{max} = 1,689 MPa)

form of dislocations), which is only possible if the diffusion of chemical components needed for reaction is strongly inhibited. Thus, new grains of unstable plagioclase may form and persist locally in a chemically isolated system on a very small scale (~1 μm).

Secondly, the observation of kyanite grains in the samples deformed to $\gamma > 3$, cannot be explained by a reaction between olivine and anorthite. Kyanite formation is observed only and typically within zones of 2 to 3 micron distance apart from olivine porphyroclasts (Fig. 9b). Taking a MgO-grain boundary diffusion rate of 2×10^{-22} $m^3 s^{-1}$ (for dry polycrystalline enstatite at 1000°C; Milke et al. (2001)), MgO can diffuse 3.5 micron in a 60 h time period, which roughly corresponds to the distance separating kyanite-rich zones from olivine porphyroclasts. This distance indicates that the diffusion rate of MgO was too low to overcome the diffusion distance between anorthite and olivine at larger strain and reaction progress. As the diffusion rates are very low in the fine-grained aggregates, it is more likely that kyanite formed by reaction of anorthite and adjacent reaction products, for example: anorthite + enstatite → kyanite + diopside. Therefore, the formation of kyanite as a local equilibrium phase is another indication of very slow diffusion.

Nucleation

Discontinuous reaction rim microstructures are often attributed to difficult (i.e. slow) nucleation of new phases (e.g. Liu et al. 1997). Such microstructures develop after 168 h at P_c =1,030 MPa in undeformed samples (Fig. 5b), and reaction has not started before ~80 h (Fig. 11a). This 'late' onset of nucleation has been observed by laboratory studies on polymorphic transformations as well, in which the equilibrium boundaries needed to be overstepped by at least 200–400 MPa before the new phases formed (Rubie 1998). The effect of additional P_c-overstep is explained by the exponential increase of the nucleation rate with the difference in Gibbs free energy (e.g. Christian 1975; Lasaga 1998) of pressure-controlled reactions. Yund (1997) has shown that the nucleation rate of enstatite reaction products is increased with confining pressure during the forsterite-quartz reaction at 900–1100°C. The enhancing effect of hydrostatic P_c-overstep on the nucleation rate is observed in our static experiments at high and low P_c-overstep, because the first reaction products nucleate after 30 h at P_c of 1,510 MPa and at ~80 h at 1,030 MPa (Fig. 11). We conclude, that the earlier reaction onset at higher P_c-overstep in the undeformed samples is a

consequence of the exponential increase of nucleation rate with confining pressure.

In the deformed samples, the grain sizes of the reaction products are one order of magnitude smaller than in the undeformed ones (compare Figs. 9a, 10a). This difference in grain size reflects a higher nucleation rate in deformed samples. The reaction products of the samples, which are initially deformed and subsequently kept at hydrostatic pressure, grow to a similar grain size (up to 3 microns) as in undeformed samples (Figs. 7, 9). The grain growth at hydrostatic pressure indicates that very little nucleation occurs after deformation has ceased.

In summary, the rim microstructures indicate that the reaction is diffusion-controlled in all studied samples and that the rates of diffusion are extremely slow due to the anhydrous conditions of the samples. It is therefore difficult to initially form reaction products in the hydrostatic experiments. Once the reaction products have formed, the reaction rate in undeformed samples will be diffusion-controlled and dominated by grain growth. In contrast, nucleation of fine-grained products continues in the deformed samples and results in higher reaction rates. We therefore suggest that an increased nucleation rate of products plays an important underlying role in the syndeformational diffusion-controlled reaction. In the following sections we will address the possible causes of the increased nucleation rates.

Potential causes for increased nucleation rates

Additional stress during deformation

Our experimentally deformed samples experience a higher 'pressure' than their equivalent hydrostatic counterparts and have a higher Gibbs free energy because of the additional differential stress. Theory predicts that locally, phase boundaries at a large angle to the highest principal stress are expected to be subjected to a higher pressure overstep than those at a small angle (Paterson 1973; Green 1986). Previous experimental studies suggest that high stresses during rock deformation may enhance phase transformations. For example, experiments on the olivine-spinel transition show an anisotropic growth of spinel nuclei during nonhydrostatic stress (Vaughan et al. 1984). Thus, in pressure-dependent reactions, it is expected that an applied differential stress contributes to the P_c-overstep and may enhance the reaction rate. Reaction products should form at high stress sites.

No orientated growth of reaction products is observed at the onset of reaction in our deformed samples (Figs. 5c, 8c). The reaction rims or patches, particularly the enstatite rims around olivine, have a uniform thickness everywhere and do not nucleate in specific locations at olivine-anorthite phase boundaries after initial deformation to small strain (Figs. 5c, 8c). At this stage of the experiment the differential stress is at its highest values (peak stress conditions; Fig. 4). The lack of preferential location, orientation, and growth of products (e.g. at high stress sites or orientations normal to the direction of principal stress σ_1) in these microstructures suggests that the nucleation of reaction products is not driven primarily by pressure overstepping due to additional differential stress.

The deformed samples in the spinel field have a σ_m^{max} ranging from 1,200 to 1,350 MPa and display an overall high reaction rate of ~0.02 ξh^{-1} (Fig. 11a). This reaction rate is considerably higher than that in the undeformed samples at higher P_c ~ 1,500 MPa (Fig. 11b), indicating that the increased reaction rate in the deformed samples cannot be explained by pressure overstepping alone. Furthermore, only 10% of the sample has reacted at peak σ_m (and σ_d; Fig. 5c). These conditions only last 6–8 h and a much larger part of the reaction progress is achieved during deformation to high strain, which takes place under decreasing and lower differential stress conditions (Figs. 4, 5). If pressure overstepping is the principal cause of enhanced reaction rates, then rates should slow down during decreasing differential stress. There is no indication for decreasing reaction rates in the deformation experiments (Fig. 11).

If the additional differential stress in the spinel-field deformation experiments is added to the pressure overstep, the resulting local stress would be high enough for the garnet stability field (Fig. 1). For example, P_c-overstepping using the σ_d^{max} of samples W1028, 19AA and 33AA corresponds to 'pressures' of 1,630, 1,720 and 1,690 MPa. Although these pressures are at least 250 MPa above the spinel-garnet transition (Fig. 1), no garnet phases have nucleated in these samples. It is unlikely that the anorthite-olivine interfaces have experienced such high stresses for sufficiently long time periods in the deforming samples to nucleate garnet as a reaction product.

From the observations and the discussion above it can be concluded that the differential stress cannot be considered as a straightforward local stress to be added to the nominal confining pressure in overstepping of an equilibrium condition. On the other hand, faster reaction rates at higher confining pressures are observed in all experiments. The differential stress probably is best accounted for as an increase of mean stress during deformation, contributing to a faster nucleation rate and to an earlier onset of reaction ('no delay') by increasing

the pressure overstep (Fig. 11a). The maximum values of σ_m are not high enough to cause the formation of garnet in experiments in the spinel field and yield pressures that are consistent with the observed phase assemblages (Fig. 1).

An average linear reaction rate of ~$0.03\xi h^{-1}$ is achieved during deformation at σ_m ranging from 1,580 to 1,800 MPa, whereas the hydrostatic reaction rate appears to decrease with time (Fig. 11b). Other mechanisms in addition to pressure overstepping are required to account for the strongly increased reaction rate in the deformed samples, which does not decrease with time. These mechanisms will be considered below.

Deformation processes

Dislocation creep of reactants The anorthite–olivine samples strain-harden until the onset of mechanical weakening in the initial stages of deformation. This hardening is probably due to inhibited dynamic recrystallisation of anorthite and olivine (i.e. strain-induced grain boundary migration) due to the presence of anorthite-olivine phase boundaries (de Ronde et al. 2005). As a result, the dislocation density in anorthite and olivine grains increases significantly while deforming the samples to maximum stress conditions. These dislocations are expected to contribute to reaction kinetics (e.g. Snow and Yund 1987).

Dislocations increase the stored strain energy of the minerals and hence their total Gibbs free energy (e.g. Wintsch and Dunning 1985). The contribution of dislocations to the total Gibbs free energy of plagioclase is ~1.0 kJ per 10^{-4} m^{-3} (Stünitz 1998), assuming a dislocation density of $10^{15} m^{-2}$. These are the highest possible values, where dislocation cores overlap and the material looses its crystalline structure. Using the Theriak software of de Capitani (1994), the total Gibbs free energy of anorthite at P_c ~ 1 GPa is ~5.6 kJ, suggesting that dislocations can account for 18% of excess free energy at most. If the contribution of dislocations to the total Gibbs free energy is expressed as a P_c-overstep (using Theriak), an additional ~40 MPa may result from the very highest dislocation densities. Thus, the bulk thermodynamic effect of dislocations on the reaction rate appears to be limited.

According to Snow and Yund (1987), deformation-induced dislocations can enhance the nucleation rate of the calcite-aragonite transformation during ductile deformation. The enhancing effect of defects (in the form of free dislocations, dislocation pile-ups and subgrain walls) on nucleation, is observed in precipitation and phase transformation in metals (e.g. Tadhani 1994; Heuser and Althauser 1997; Hamana et al. 1998; Levitas 2004) and in earth materials (e.g. Liu and Yund 1995; Kubo et al. 1998; Dupas-Bruzek et al. 1998; Kerschhofer et al. 2000). The defects and distorted lattices serve as nucleation sites, similar to brittle deformation features (e.g. Baronnet and Belluso 2002; Stünitz et al. 2003). The enhancing nature of defects on the nucleation rate appears to be a local effect, which is particularly important at grain boundaries where the defect densities are highest because of high stresses. The local high defect densities at grain boundaries, dislocation pile-ups, and subgrain walls are not readily expressed as a bulk thermodynamic property.

It should be emphasised that when it is argued that local high dislocation densities are responsible for increased nucleation rates, this explanation is not fundamentally different from an explanation of applying a differential stress, because the applied stress initially causes the local high dislocation densities. However, reaction and viscous deformation continuously change the local stress field at the phase/grain boundaries of deforming aggregates, and therefore differential stress cannot be used as a straightforward explanation for the observed effects. In a deforming polycrystalline aggregate, plastic strain energy in the form of dislocations exceeds an elastic energy contribution by far and is the principal cause for an increase in Gibbs energy (e.g. Paterson 1973; Poirier 1985).

The effect of high dislocation densities on the nucleation rate is consistent with our observations, because dislocations are generated by applying a differential stress to the samples. Once differential stress is removed from deforming samples in our combined deformation-static experiments, reaction rates decrease to values characteristic for undeformed samples (Fig. 11). The contribution of dislocations is only important during active dislocation creep processes. Unfortunately, the effect is difficult to asses more quantitatively with the data presented here.

Granular flow of reaction products The syndeformational reaction products accommodate deformation by granular flow (i.e. non-frictional grain boundary sliding) and are finer grained compared to undeformed products (Fig. 9b). The effect of the relative movement of products by granular flow becomes important once foliation structures start to develop after the onset of the mechanical weakening (i.e. after σ_m^{max}, towards larger strain). Granular flow and the small grain size of the syndeformational products can exert a control on the reaction.

The neighbour switching of product grains during granular flow may disturb the two-layer reaction rim

geometry. The removal of products from the anorthite-olivine reaction interfaces is illustrated by the lobate enstatite rim and tail microstructures (Fig. 9b). In undeformed samples, rims thicken by grain growth, decreasing the chemical gradient and hence the reaction rate. In deformed samples, reaction rims become mixed and locally narrower (Figs. 5d, 8d), which helps to sustain the chemical gradient normal to the rims and in the shortening direction. This effect enhances the diffusion and possibly the nucleation rate of reaction products.

Secondly, granular flow leads to an increased dispersion of phases (Kruse and Stünitz 1999; Kenkmann and Dresen 2002), and therefore suppresses grain growth during deformation by grain boundary pinning (e.g. Olgaard and Evans 1988). Intensive mixing and short diffusion distances are known to increase reaction kinetics during ball milling and deformation in many materials as well (e.g. Tadhani 1994; Battezzati et al. 1999). Granular flow helps the diffusion distances to remain short in certain orientations and it maintains small grain sizes.

Both of the described effects are deformation- and not stress-dependent. Thus, the deformation-enhanced reaction rate can be obtained in two ways. (1) Deformation at elevated mean stress at small strain (resulting in high dislocation densities) contributes to the pressure overstep of equilibrium conditions. (2) Granular flow of reaction products to large strains during the mechanical weakening maintains a high chemical potential and a small grain size of products. All of these enhance the nucleation rate of products and therefore increase the reaction rate during deformation.

Geological applications

Deformation of the anorthite–olivine aggregates causes increased nucleation and reaction rates. A straightforward interpretation of the reaction in terms of diffusion parameters is difficult, because nucleation and length scales of reaction in deformed rocks may be very different from undeformed cases. Reaction rates from hydrostatic experiments provide only minimum values if extrapolated to nature. The deformation and reaction experiments point to several general implications for simultaneous deformation and reaction processes in natural systems.

Most importantly, the faster reaction rate during viscous deformation of An–Fo aggregates is obtained at anhydrous conditions. Therefore, significant infiltration of water into ductile shear zones is not a prerequisite for the localisation of metamorphic reactions. This result agrees with conclusions of Kerrich et al. (1980), who observed that the localisation of reaction in granitoid mylonites was not associated with high fluid fluxes. An increase in reaction rate in nature may be caused by viscous deformation itself, and not necessarily by fluid infiltration.

Metastable phases may form when reactions occur at conditions of large P_c-overstepping due to a impeded nucleation (e.g. Rubie 1998). Despite the large P_c-overstep in our hydrostatic experiments (ranging from 300 to 800 MPa), no metastable phases were identified in the reaction products. Deformation at shear strains above $\gamma = 3$ at P_c =1,630 MPa did result in metastable kyanite as a consequence of the reaction rate being faster than the diffusion rate of components needed for the reaction. Thus, a higher nucleation rate during deformation can cause the formation of local metastable phases that may not be part of the equilibrium assemblage.

The reversal of the investigated reaction is often observed in natural mylonitic shear zones in extensional tectonic settings, where mantle rocks are adiabatically brought up to shallower levels in the crust and become chemically unstable (Furusho and Kanagawa 1999; Newman et al. 1999; Handy and Stünitz 2002). The pressure–temperature range of the experiments is realistic for such upper mantle shear zones. Although natural deformation takes place at lower strain rates ($10^{-12} \sim 10^{-14}$ s^{-1}) and stresses, the deformation of upper mantle rock can take place by dislocation creep mechanisms due to the larger grain sizes (e.g. sizes >100 μm in peridotite proto-mylonites (Newman et al. 1999; Handy and Stünitz 2002)).

In naturally deforming rocks, lower stresses and strain rates are reflected in the lower build-up of dislocations in minerals. However, grain-scale stress concentrations in minerals will always lead to a local increase of dislocation densities. Subgrain walls and pile-ups, as a result of differential stress, are common in natural systems so that it is expected that the enhancement of reaction by crystal plastic deformation in nature is as important as in our experiments. The effect of relative displacement of reactants and products are likely to have a more important contribution in naturally deforming rocks that deform at lower stresses. Thus, the results of our experiments have a direct application to natural cases of syndeformational reaction, especially in metamorphosed rocks during deformation at fluid-deficient conditions.

The initiation and continuation of shear localisation in the dry lower crust and upper mantle are important for the accommodation of tectonic movements during crustal thinning and extension (e.g. Vissers et al. 1995).

Basement rocks can be dry for long periods of time under metamorphic conditions with only short and localised periods of fluid infiltration (Rubie 1986). The enhancement of reaction by viscous deformation under dry conditions (e.g. reaction overstepping, build-up of dislocation densities and mechanical displacement of fine-grained material) may greatly contribute to shear localisation in the dry lower crust and upper mantle.

Conclusions

We have studied the effects of viscous deformation processes on the kinetics of a diffusion-controlled reaction between anorthite and olivine at dry conditions. For this purpose, we performed deformation experiments in shear and hydrostatic experiments on anhydrous plagioclase-olivine aggregates at 900°C and confining pressures of 1,000–1,600 MPa. The following conclusions are made:

- At hydrostatic pressure, the formation of reaction rims indicates that reaction between anorthite and olivine is diffusion-controlled. The dry conditions in the studied samples result in slow diffusion rates of chemical components.
- Increased mean stress and viscous deformation processes of the reactants and products enhance the rate of reaction in An–Fo aggregates at water-deficient conditions. The enhanced reaction rate in the deforming samples is caused by an increase of the nucleation rate of reaction products.
- The increased nucleation rate in the deforming samples is mainly attributed to two processes. At low shear strains ($\gamma;\lesssim 3$), high mean stresses cause the build-up of high dislocation densities in the reactants, particularly at grain boundaries and locally contribute to the Gibbs free energy of the assemblage. The increased Gibbs free energy of the assemblage causes a faster nucleation rate. From the onset of mechanical weakening towards larger shear strain, the removal of products from the reaction interfaces at the olivine and anorthite grain boundaries by granular flow may maintain high chemical potentials and may cause continued nucleation of fine-grained reaction products.
- During deformation at differential stress, the low diffusion rates of chemical species, combined with fast nucleation rates of reaction products, results in the local formation of metastable kyanite, which is not part of the equilibrium assemblage.

Acknowledgments We are thankful to Georg Dresen and an anonymous reviewer for their extensive and constructive reviews. We gratefully acknowledge Jan Tullis and Renée Heilbronner for their help with improving the manuscript. We thank Ralph Milke and Rainer Abart for discussion on diffusion-controlled reactions. Christian de Capitani and Phillipe Hunziker are thanked for their help with petrological calculations.

References

Austrheim H (1987) Eclogitization of lower crustal granulites by fluid migration through shear zones. Earth Planet Sci Lett 81(2–3):221–232

Baronnet A, Belluso E (2002) Microstructures of the silicates: key information about mineral reactions and a link with the Earth and material sciences. Min Mag 66:709–732

Battezzati L, Pappalepore P, Durbiano F, Gallino I (1999) Solid state reactions in Al/Ni alternate foils induced by cold rolling and annealing. Acta Mat 47:1901–1914

Berman RG (1988) Internally-consistent thermodynamic data for minerals in the system Na_2O–K_2O–CaO–MgO–FeO–Fe_2O_3–Al_2O_3– SiO_2–Ti O_2–H_2O–CO_2. J Petrol 29(2):445–522

Brodie KH, Rutter EH (1985) On the relationship between deformation and metamorphism, with special reference to the behaviour of basic rocks. In: Thompson AB, Rubie DC (eds) Metamorphic Reactions: Kinetics, Textures and Deformation. Springer, New York, pp 138–179

Brodie KH, Rutter EH (1987) The role of transiently fine-grained reaction products in syntectonic metamorphism: natural and experimental examples. Can J Earth Sci 24:556–564

Burnley PC, Green HW (1989) Stress dependence of the mechanism of the olivine-spinel transformation. Nature 338(6218):753–756

de Capitani C (1994) Gleichgewichtsphasendiagramme: Theorie und software. Eur J Mineral 6:48–50

de Capitani C, Brown TH (1987) The computation of chemical equilibrium in complex systems containing non-ideal solutions. Geochim Cosmochim Ac 51(10):2639–2652

Christian JW (1975) The Theory and Transformation In Metals and Alloys. Pergamon Press, Oxford

Davis BL, Adams LH (1965) Kinetics of the calcite-aragonite transformation. J Geophys Res 70(2):433–441

Dupas-Bruzek C, Sharp T, Rubie D, Durham W (1998) Mechanisms of transformation and deformation in $Mg_{1.8}Fe_{0.2}SiO_4$ olivine and wadsleyite under non-hydrostatic stress. Phys Earth Planet In 108:33–48

Fisher GW (1978) Rate laws in metamorphism. Geochim Cosmochim Ac 42(7):1035–1050

Früh-Green G (1994) Interdependence of deformation, fluid infiltration and reaction progress recorded in eclogitic metagranitoids (Sesia Zone, W. Alps). J Metamorph Geol 12:327–343

Fuhrman ML, Lindsley DH (1988) Ternary-feldspar modelling and thermometry. Am Mineral 73:201–215

Furusho M, Kanagawa K (1999) Transformation-induced strain localization in a lherzolite mylonite from the Hidaka metamorphic belt of central Hokkaido, Japan. Tectonophysics 313(4):411–432

Gasparik T (1984) Two-pyroxene thermobarometry with new experimental data in the system CaO-MgO-Al_2O_3-SiO_2. Contrib Mineral Petr 87(1):87–97

Green II HW (1986) Phase transformation under stress and volume transfer creep. In: Hobbs BC, Heard HC (eds) Minerals and rock deformation: laboratory studies, The Paterson volume, vol 36, AGU Geophys. Monogr., pp 201–211

Green DH, Hibberson W (1970) The instability of plagioclase in peridotite at high pressure. Lithos 3:209–221

Hamana D, Bouchear M, Derafa A (1998) Effect of plastic deformation on the formation and dissolution of transition phases in Al-12 wt.%-Mg alloy. Mat Chem Phys 57:99–110

Handy MR, Stünitz H (2002) Strain localization by fracturing and reaction weakening—a mechanism for initiating exhumation of subcontinental mantle beneath rifted margins. In: de Meer S, Drury MR, de Besser JHP, Pennock GM (eds) Deformation mechanisms, rheology and tectonics: current status and future perspectives, vol 200, Geol. Soc. Spec. Pub., pp 387–407

Heuser B, Althauser J (1997) Effect of deformation on low-temperature deuteride precipitation in single crystal niobium. J Phys Condens Matter 9:8945–8961

Hunziker P (2003) The stability of tri-octahedral Fe^{2+}-Mg-Al chlorite. A combined experimental and theoretical study. PhD thesis, Basel University

Jenkins DM, Newton RC (1979) Experimental determination of the spinel peridotite to garnet peridotite inversion at 900°C and 1000°C in the system CaO–MgO–Al_2O_3–SiO_2, and at 900°C with natural garnet and olivine. Contrib Mineral Petrol 68(4):407–419

Joesten R (1978) Diffusion-controlled growth of pyroxene-spinel coronas between forsterite and anorthite in the system CaO–MgO–Al_2O_3–SiO_2. Geol Soc Am Abstr Program 10:429

Joesten R (1991) Grain-boundary diffusion kinetics in silicate and oxide minerals. In: Ganguly J (ed) Diffusion, atomic ordering and mass transport. Springer, Heidelberg, pp 347–397

John T, Schenk V (2003) Partial eclogitisation of gabbroic rocks in a late Precambrian subduction zone (Zambia); prograde metamorphism triggered by fluid infiltration. Contrib Mineral Petrol 146(2):174–191

Keller LM, Abart R, Stuenitz H, de Capitani C (2004) Deformation, mass transfer and mineral reactions in an eclogite facies shear zone in a polymetamorphic metapelite (Monte Rosa Nappe, Western Alps). J Metamorph Geol 22(2):97–118

Kenkmann T, Dresen G (2002) Dislocation microstructure and phase distribution in a lower crustal shear zone—an example from the Ivrea-Zone, Italy. Int J Earth Sci 91(3):445–458

Kerrich R, Allison J, Barnett RL, Moss S, Starkey J (1980) Microstructural and chemical transformations accompanying deformation of granite in a shear zone at Miéville, Switzerland; with implications for stress corrosion cracking and superplastic flow. Contrib Mineral Petrol 73(3):221–242

Kerschhofer L, Rubie D, Sharp T, McDonnell J, Dupas-Bruzek C (2000) Kinetics of intracrystalline olivine-ringwoodite transformation. Phys Earth Planet In 121:59–76

Kirby SH, Stern LA (1993) Experimental dynamic metamorphism of mineral single crystals. J Struct Geol 15(9–10):1223–1240

Klemme S, O'Neill HSC (2000) The near-solidus transition from garnet lherzolite to spinel lherzolite. Contrib Mineral Petrol 138(3):237–248

Kruse R, Stünitz H (1999) Deformation mechanisms and phase distribution in mafic high- temperature mylonites from the Jotun Nappe, southern Norway. Tectonophysics 303(1–4):223–249

Kubo T, Ohtani E, Kato T, Shinmei T, Fujino K (1998) Experimental investigation of the α – β-transformation of San Carlos olivine single crystal. Phys Chem Minerals 26:1–6

Kushiro I, Yoder HS (1966) Anorthite-forsterite and anorthite-enstatite reactions and their bearing on the basalt-eclogite transformation. J Petrol 7(3):337–362

Lasaga AC (1998) Kinetic Theory in the Earth Sciences. Princeton University Press, New Jersey

Levitas V (2004) Strain-nucleation at a dislocation pile-up: a nanoscale model for high pressure mechanochemistry. Phys Let A 327:180–185

Liu M, Yund R (1995) The elastic strain energy associated with the olivine-spinel transformation and its implications. Phys Earth Planet In 89:177–197

Liu M, Peterson JC, Yund RA (1997) Diffusion-controlled growth of albite and pyroxene reaction rims. Contrib Mineral Petrol 126(3):217–223

Marquer D, Gapais D, Capdevila R (1985) Comportement chimique et orthogneissification d'une granodiorite en facies schistes verts (Massif de l'Aar, Alpes Centrales). B Mineral 108(2):209–221

Meyre C, de Capitani C, Partzsch JH (1997) A ternary solid solution model for omphacite and its application to geothermobarometry of eclogites from the Middle Adula Nappe (Central Alps, Switzerland). J Metamorph Geol 21(8):813–829

Milke R, Wiedenbeck M, Heinrich W (2001) Grain boundary diffusion of Si, Mg, and O in enstatite reaction rims: a SIMS study using isotopically doped reactants. Contrib Mineral Petrol 142(1):15–26

Newman J, Lamb WM, Drury MR, Vissers RLM (1999) Deformation processes in a peridotite shear zone: reaction-softening by an H_2O-deficient, continuous net transfer reaction. Tectonophysics 303(1–4):193–222

Olgaard DL, Evans B (1988) Grain growth in synthetic marbles with added mica and water. Contrib Mineral Petrol 100(2):246–260

O'Neill HSC (1981) The transition between spinel lherzolite and garnet lherzolite, and its use as a barometer. Contrib Mineral Petrol 77(2):185–194

Paterson MS (1973) Non-hydrostatic thermodynamics and its geological applications. Rev Geophys Space Phys 11:355–389

Poirier JP (1985) Creep of Crystals: High-temperature Deformation Processes in Metals, Ceramics and Minerals. Cambridge University Press, Cambridge

de Ronde AA, Heilbronner R, Stünitz H, Tullis J (2004) Spatial distribution of deformation and mineral reaction in experimentally deformed plagioclase-olivine aggregates. Tectonophysics 389(1–2):93–109

de Ronde AA, Stünitz H, Tullis J, Heilbronner R (2005) Reaction-induced weakening of plagioclase-olivine composites. Tectonophysics 409:85–106

Rubie DC (1983) Reaction-enhanced ductility: the role of solid-solid univariant reaction in deformation of the crust and mantle. Tectonophysics 96(3–4):331–352

Rubie DC (1986) The catalysis of mineral reactions by water and restrictions on the presence of aqueous fluid during metamorphism. Min Mag 50:399–415

Rubie DC (1998) Disequilibrium during metamorphism: the role of nucleation kinetics. In: Treloar PJ, O'Brien PJ (eds) What drives metamorphism and metamorphic reactions, vol 138, Geol. Soc., Spec. Pub., pp 199–214

Snow E, Yund RA (1987) The effect of ductile deformation on the kinetics and mechanisms of the aragonite-calcite transformation. J Metamorph Geol 5(2):141–153

Stünitz H (1998) Syndeformational recrystallisation: dynamic or compositionally induced? Contrib Mineral Petrol 131(2–3):219–236

Stünitz H, FitzGerald JD, Tullis J (2003) Dislocation generation, slip systems, and dynamic recrystallization in experimentally deformed plagioclase single crystals. Tectonophysics 372(3–4):215–233

Tadhani N (1994) Shock-induced and shock-assisted solid-state chemical reactions in powder mixtures. J App Phys 76:2129–2138

Underwood EE (1970) Quantitative stereology. Addison-Wesley Publishing Company, Reading, Mass

Vaughan PJ, Green HW, Coe RS (1984) Anisotropic growth in the olivine-spinel transformation of Mg_2GeO_4 under non-hydrostatic stress. Tectonophysics 108(3–4):299–322

Vissers RLM, Drury MR, Hoogerduijn Strating EH, Spiers CJ, van der Wal D (1995) Mantle shear zones and their effect on lithosphere strength during continental break-up. Tectonophysics 249(3-4):155–171

White SH, Knipe RJ (1978) Transformation- and reaction enhanced ductility in rocks. J Geol Soc London 135:513–516

Wintsch RP, Dunning J (1985) The effect of dislocation density on the aqueous solubility of quartz and some geologic implications: a theoretical approach. J Geophys Res 90(5):3649–3657

Yund RA (1997) Rates of grain boundary diffusion through enstatite and forsterite reaction rims. Contrib Mineral Petrol 126(3):224–236